Paliperidone palmitate as model of heat-sensitive drug for long-acting 3D printing application

Giuseppe Manini [a,b,*], Samira Benali [b], Allen Mathew [c], Simone Napolitano [c], Jean-Marie Raquez [b], Jonathan Goole [a]

[a] *Laboratory of Pharmaceutics and Biopharmaceutics, Université libre de Bruxelles, Campus de la Plaine, CP207, Boulevard du Triomphe, Brussels 1050, Belgium*
[b] *Laboratory of Polymeric and Composite Materials (LPCM), Center of Innovation and Research in Materials and Polymers (CIRMAP), University of Mons, Place du Parc 23, B-7000 Mons, Belgium*
[c] *Laboratory of Polymer and Soft Matter Dynamics, Experimental Soft Matter and Thermal Physics (EST), Université libre de Bruxelles (ULB), Boulevard du Triomphe, Bruxelles 1050, Belgium*

ABSTRACT

In this work, two technologies were used to prepare long-acting implantable dosage forms in the treatment of schizophrenia. Hot-melt extrusion (HME) as well as fused deposition modelling (FDM) were used concomitantly to create personalized 3D printed implants. Different formulations were prepared using an amorphous PLA as matrix polymer and different solid-state plasticizers. Paliperidone palmitate (PP), a heat sensitive drug prescribed in the treatment of schizophrenia was chosen as model drug. After extrusion, different formulations were characterized using DSC and XRD. Then, an *in vitro* dissolution test was carried out to discriminate the formulation allowing a sustained drug release of PP. The formulation showing a sustained drug release of the drug was 3D printed as an implantable dosage form. By modulating the infill, the release profile was related to the proper design of tailored dosage form and not solely to the solubility of the drug. Indeed, different release profiles were achieved over 90 days using only one formulation. In addition, a stability test was performed on the 3D printed implants for 3 months. The results showed the stability of the amorphous state of PP, independently of the temperature as well as the integrity of the matrix and the drug.

1. Introduction

Nowadays, pharmaceutical companies are facing to a real paradigm to develop efficient and scalable methods to meet the demand of personalized dosage forms. In this respect, three-dimensional printing (3DP) represents a suitable technique to fulfil such requests, while enabling high manufacturing versatility at relatively low cost. For more than 30 years, the interest in 3D printing has been growing and is being still considered as a realistic scalable manufacturing technique (Prasad and Smyth, 2016). In the early '90s, the 3D printing process, particularly the Solid Freeform Fabrication (SFF) developed at MIT (Cambridge, MA) (Sachs et al., 1993), led to the creation of structured and tailored drug delivery systems. In 2015, the approval of the first marketed 3D printed fast-disintegrating tablets (Spritam®) by the Food and Drug Administration (FDA) highlighted the industrial interest to implement 3D-printing in the pharmaceutical realm. Another industrial motivation is related with the large range of 3D-printing techniques available for the pharmaceutical field, enclosing the Powder-based printing (Infanger et al., 2018), Stereolithography (SLA) (Xu et al., 2020), Selective Laser Sintering (SLS) (Fina et al., 2017), Pressure-Assisted Microsyringe

---

(PAM) (El et al., 2020) and Fused Deposition Modeling (FDM) (Pietrzak et al., 2015).

Among these plethoric 3D-printing techniques, FDM process is the most represented 3D printing technology in the literature (Azad et al., 2020). This process is based on the use of a thermoplastic filament containing the active ingredient, which is pushed by two gears in a heated barrel and extruded through a nozzle. Then, the molten polymer is applied layer-by-layer to create the final product (Goyanes et al., 2017). This low-cost process may be easily developed for several applications such as the development of implantable dosage forms (Kempin et al., 2017). This 3D printing process is so versatile, allowing to modulate the shape, the volume, the weight as well as the micro-architecture to create tailored implantable devices based on only one single formulation (Kempin et al., 2017; Jonathan and Karim, 2015).

The use of polymers for 3D printing opens a wide range of possibilities to adapt the release profile of a loaded drug. For that purpose, most popular thermoplastic materials used in FDM are described to be poly-lactic acid (PLA) (Kempin et al., 2017), polycaprolactone (PCL) (Kempin et al., 2017), polyvinyl alcohol (PVA) (Azad et al., 2020); poly(lactic-co-glycolic acid) (PLGA) (Feuerbach et al., 2019), and ethylene–vinyl acetate (EVA) (Lim et al., 2018; Genina et al., 2016).

However, such polymers need to be formulated and extruded as drug-loaded printable filaments before being 3D printed as drug delivery systems (DDS). The first drug-loaded filaments were obtained by soaking a commercial filament made of PVA in an ethanolic solution made of drug (Goyanes et al., 2014). However, this technique was not considered as efficient enough due to the very low yield in loading even if a high amount of drug was initially involved.

Therefore, *Goyanes et al.* described a protocol based on Hot-Melt Extrusion (HME) to produce printable drug-loaded filaments. Using HME, the active pharmaceutical ingredient (API) and excipients are blended in a heated barrel and conveyed by two screws and extruded through a die (Goyanes et al., 2015). Such method allows producing a homogeneous dispersion of the API into a polymeric printable filament characterized by an adapted diameter for the use of FDM.

This technology may be also useful to produce amorphous solid dispersions (ASD). The heat and the shear applied during the process allow stabilizing the drug under its amorphous state within the polymer matrix (Simões et al., 2019). Like HME, 3D printing by FDM is also based on a thermal process that allows obtaining an amorphous form of a loaded API (Goyanes et al., 2019). Stabilizing molecules into their amorphous state by using a non-solvent process is an adequate solution as most of new molecules have a poor water solubility and a high permeability. Moreover, the use of a non-solvent process facilitates the manufacturing of such dosage form. Therefore, combining HME and FDM offers novel opportunities to develop DDS loaded with amorphous API and characterized by adapted shapes and volumes for a better patient acceptability (Goyanes et al., 2017).

In this work, Paliperidone Palmitate (PP) was selected as a model drug. This API is a marketed pro-drug widely used for the treatment of schizophrenia. As already mentioned by *Brissos et al,* especially in the framework of psychotic pathologies, the use of dosage forms with prolonged release has already shown their added value such as a reduction of the administrated dose and a lower risk of over consumption (Brissos et al., 2014). As also pointed out by *Jose de Leon,* the doses available for this type of pathology are determined for an ideal average patient (de Leon, 2020). Therefore, there is a real need to tailor the dosage to the needs of each patient.

PP is already available as long-acting injectable dosage form and after administration, the API is hydrolyzed into palmitic acid and its active drug, the paliperidone (9-hydroxyrisperidone) (Leng et al., 2014). PP is characterized as practically insoluble in water (intrinsic solubility below 0.1 µg/ml) (Remenar, 2014; Janssen, 2017) and a melting point of around 115 °C (Leng et al., 2014). Nowadays, PP is formulated as nanocrystals. Therefore, its dissolution profile is mainly determined by its own solubility. However, as shown by *Darville et al,* the large amounts

of crystalline PP presents in this kind of formulation may initiate a chronic granulomatous inflammatory reaction (Darville et al., 2014). A solution to avoid this issue could be to disperse the drug into a polymer matrix. *Nanaki et al* used a high surface area mesoporous silica foam to enhance the solubility of paliperidone, the parent molecule of PP. This foam was encapsulated in PLA and PLGA as microparticles to sustain the release of the drug from 10 to 15 days (Nanaki et al., 2017). More recently*, Elmowafy et al* have developed a paliperidone-loaded poly-caprolactone-based (PCL) nanoparticles and investigated the influence of different stabilizers as well as the presence of a coating and the PCL/drug ratio (Elmowafy et al., 2020). As it can be seen, most of these studies were focused on the physicochemical modification of the API alone and/or the development of drug-loaded microspheres. An alternative to the development of polymeric microspheres could be the use of HME to produce and stabilize the amorphous form of PP into printable filaments to develop potential personalized implantable DDS in the treatment of schizophrenia. Implantable dosage forms can be an interesting alternative, especially for patients with a poor medication adherence (Stewart et al., 2020). They have already been investigated to prevent breast cancer recurrence (Hao et al., 2021), for the prevention of cardiovascular thrombosis (Domínguez-Robles et al., 2021) or even for the treatment of intravesical disease (Xu et al., 2021). Nevertheless, both HME and 3D printing may be considered as deleterious techniques for the loaded PP due to the shear stress as well as the use of relative high temperatures. Therefore, the influence of these parameters must be evaluated as they are well-known to be limiting factors to produce stable dosage forms (Simões et al., 2019; Ilyés et al., 2019). In the literature, there are few articles focusing on stability and degradation products of the PP. By referring to the work carried out on parents' molecules of PP, namely paliperidone and risperidone, interesting information has been found. *Trivedi et al,* have shown that PP is sensitive to oxidation (Trivedi et al., 2013). *Selmin et al,* shown that tertiary amines contained in risperidone accelerate the degradation of PLGA (Selmin et al., 2012). *Bharathi et al,* have also shown that heating and light can induce a rearrangement of the oxazole ring present in risperidone (Bharathi et al., 2008).

In this paper, these parameters were considered to select the best polymers and excipients which may be processed at the lowest temperatures. Printable filaments allowing different release profiles of PP were obtained, depending on the matrix and the 3D design without the generation of any degradation products. In this paper, PLA was selected for its mechanical properties (Tümer and Erbil, 2021), ease to prepare adapted filaments for FDM and allowing a sustain release of PP over-time. Moreover, it is an FDA-approved polymer for human use (Li et al., 2013). To decrease its processing temperature, different excipients were investigated such as polyethylene glycol or Poloxamer for their ability to act as plasticizer, but also EVA for its hydrophobicity and low processing temperature. After processing the different formulations by HME, the printable filaments were screened through an *in vitro* dissolution test. The formulation displaying a sustain release of PP overtime was chosen to prepare tailored 3D printed dosage form. Based on the chosen ternary mixture, different release profiles of PP were obtained, depending on the 3D design without the generation of any degradation products. Moreover, the amorphous state of PP obtained by the successive processes has shown to be stable along stability tests.

2. Materials and experimental part

2.1. Materials

PLA 4060D, amorphous PLA with 12% D-Lactide (M_w = 239,000 g/mol), was purchased from Ingeo NatureWorks® (USA), EVA 233 with 23% of vinyl acetate content (ρ = 0.947 g/cm^3) was purchased from Exxon Mobil Chemical Company® (USA). Paliperidone palmitate was purchased from Biochem Partner (China), Polyethylene glycol 2000 (PEG2000) was purchased from Sigma-Aldrich® (USA), Poloxamer®

188 (P188) was kindly donated by BASF® (Germany). Trifluoroacetic acid, chloroform, chloride methylene, acetonitrile and isopropanol were purchased from Sigma-Aldrich® (USA). Hydrochloric acid and Tween® 20 were purchased from VWR® (USA).

2.2. Preparation of amorphous solid dispersions and evaluation

2.2.1. Hot-Melt extrusion

As PLA is usually extruded at a temperature of around 180 °C, i.e., close to the degradation temperature of PP, the direct preparation of a polymer-excipient-API mixture cannot be carried out in a single step process. Therefore, it was necessary to plasticize PLA during a pre-formulation step. This first blending step was made using an internal blender (Brabender© model 50 EHT (Brabender© GmbH&Co)). This step was performed on 40 g in sample:

After this step, the resulting materials were coarsely ground with an IKA® A10 mill (Werke GmbH & Co©, Staufen) to facilitate its milling.

2.2.2. Cryomilling

Cryogenic milling was conducted in an oscillatory Retsch® Cryomill (Retsch GmBH©, Haan, Germany). The formulations were placed in a 25 ml stainless steel grinding jar with 3 stainless steel beads of 15 mm. The milling time was divided into different cycles of 2 min at 30 Hz and different cycles of 30 s at 5 Hz to avoid any overheating. The cryogenic milling was carried out on formulations to reduce the aggregates into powder. Then, formulations were passed through a 40 mesh sieve.

2.2.3. Preparation of drug loaded filament by melt extrusion

Filaments loaded with 10 % w/w of PP were prepared by HME using a parallel twin-screw extruder (Thermo Scientific® Process 11, Thermo Fisher Scientific Inc.®, USA) with 8 separate heating zones, including the die (ø = 1.75 mm). Temperature, die pressure, torque, and speed of rotation of the screws were continuously monitored. The speed of the screws was fixed at 30 rotations per minute (RPM). The temperature of the different heating zones was fixed as follow (from zone 1 to zone 8): 60/80/125/125/125/125/125/110 °C. A volumetric feeder (Volumetric Mini Twin-Feeder, Thermo Fisher Scientific Inc.®, USA) was used to convey the formulations into the extruder and the screw speed of the feeder was set at 5 RPM (2.5 g/min). After extrusion, the filaments were collected using a filament winder to obtain a diameter of 1.75 ± 0.1 mm.

2.2.4. Thermal analysis

Differential scanning calorimetry (DSC) was conducted with a DSC Q2000 with T_{zero} Technology and RCS cooling system. Temperature and enthalpy calibrations were performed using an indium standard (TA Instruments®, New Castle, USA). Approximately 5–10 mg of samples were sealed in T_{zero} hermetic aluminum pan. The samples were heated from −50 °C to 130 °C with a heating rate of 10 °C/min. All analyses were conducted under nitrogen atmosphere (50 ml/min).

Thermal decomposition of samples was assessed by thermogravimetric analysis (TGA). The analysis was performed with a TGA Q500 (TA Instruments®, New Castle, USA). Samples of 5–10 mg were loaded into a platinum pan and were heated from 30 to 450 °C with a heating rate of 10 °C/min under nitrogen gas (flow rate: 60 ml/min).

2.2.5. Gel permeation chromatography

Gel permeation chromatography (GPC) analysis was conducted on an Agilent liquid Chromatography (Agilent Technologies®, United States) equipped with an Agilent degasser, an isocratic HPLC pump with a flow rate set at 1 ml/min. Chloroform was used as mobile phase and polystyrene were used as standards for calibration. The GPC was equipped with an Agilent autosampler, the loop volume was 100 μL. The solutions were concentrated at 2 mg/ml. The GPC was equipped with an Agilent DRI refractive index detector and three columns: a PL gel 5 mm guard column (Polymer Laboratories®, Ltd, United Kingdom) and two PL gel Mixed-B 5 μm columns (columns for separation of polystyrene

with a Mw ranging from 200 to $4x10^5$ g/mol) were used at 30 °C to evaluate the M_w of samples.

2.2.6. X-Ray powder diffraction

A powder X-Ray diffractometer (D8 Advance Eco Bruker®, Madison, USA) equipped with a one-dimensional silicon detector (LynxEye, Bruker AXS) was used to characterize the crystalline/amorphous structure of PP, starting elements and formulations. Using a Cu Kα radiation (1.54 Å; 40 kV × 25 mA) data were collected, over the angular range of 3–45° 2θ and a step size of 0.02° and a dwell time of 1 s.

2.2.7. Determination of drug loading

To extract the API, samples loaded with an average weight of 1 mg of API were solubilized in 1 part of chloride methylene under vortex until its complete solubilization. Then, 9 parts of isopropanol were added drop by drop under vortex. Solutions were filtered through 0.22 μm filters (Sortorius®) and filled in 2 ml vial for HPLC analysis.

An HPLC-UV method was conducted to evaluate the drug loading from the extruded filaments as well as from 3D implants. Mobile phase A, which consisted of acetonitrile (100 % v/v), and mobile phase B (aqueous solution of trifluoroacetic acid at pH 2) were used at ratio 70/30 A/B (v/v). The flow rate was set at 1 ml/min for 20 min and the wavelength was fixed 278 nm. The retention time of PP was 8.0 min.

2.2.8. Dielectric spectroscopy

Different formulations were studied using dielectric spectroscopy. The samples in the form of extruded films were placed between two brass electrodes and measured under an inert atmosphere of helium. Measurements of electric impedance were performed within the frequency range from 1 Hz to 1 MHz at different fixed temperatures, from 30 to 140 °C with a 2 °C step, via a ModuLab XM MTS, Solartron Analytical© (Ametek, United-Kingdom). The sample temperature was precisely controlled using a cryostat and a proportional–integral–derivative (PID). The complex dielectric constant (ε), which is a function of frequency (ω) and temperature (T), was analyzed using the empirical Havriliak–Negami (HN) (1) equation as given by:

$$\varepsilon(\omega, T) = \varepsilon_\infty + \left[\frac{\Delta\varepsilon}{(1 + (i\omega\tau_{HN})^\alpha)^\beta} \right]$$

where $\Delta\varepsilon$ and τ_{HN} are the dielectric strength and the HN characteristic time, ε_∞ is the high frequency permittivity and τ is the relaxation time. α and β are the shape parameters, respectively, related to the width and the asymmetry of the loss curves. The position of the maximum of the relaxation peak was, hence, obtained as

$$\omega_{max} = \frac{1}{\tau_{HN}} \left[sin \frac{\alpha\pi}{2 + 2\beta} \right]^{\frac{1}{\alpha}} \left[sin \frac{\alpha\beta\pi}{2 + 2\beta} \right]^{-\frac{1}{\alpha}}$$

Via a model free approach, the segmental relaxation time τ is related to the maximum of the relaxation peak as $\tau\omega_{max} = 1$. Glass transition temperature (T_g) was calculated by fitting the temperature evolution of relaxation time (τ) using the Vogel-Fulcher-Tammann (VFT) Eq. (2), given by:

$$\tau = \tau_\infty exp\left(\frac{DT_0}{T - T_0} \right)$$

where, τ_∞ and D are constants and T_0 is called Vogel temperature. Though it was not possible to follow the segmental process down to frequencies lower than 1 Hz, the dynamic glass transition temperature was obtained by extrapolating the temperature dependence of τ down to the temperature at which the segmental time reaches 100 s.

2.2.9. Design software

Tinkercad® was used as computer aided design (CAD) program to design the geometry of our implantable dosage forms (Fig. 1). The
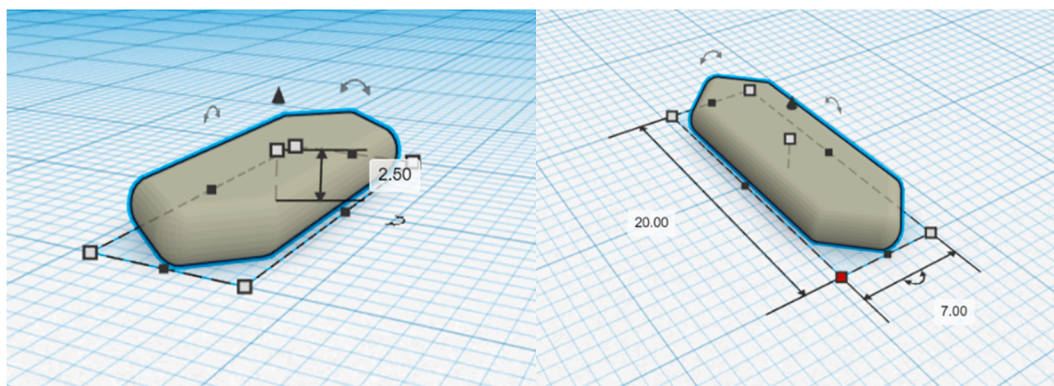
Fig. 1. Dimensions of the implantable device: 20 mm / 7 mm / 2.5 mm, L / W / H.

generated CAD files were converted into .stl files. Then, the obtained files were imported into an open-source software for slicing before printing. Slic3r® 1.3.0, was used to generate .gcode files compatible with the 3D printer.

2.2.10. 3D printing

FDM was conducted on a Hyrel® system 30 M (Norcross, USA), equipped with a MK1 head adapted to 1.75 mm diameter printable filament and a nozzle head of 0.4 mm diameter. The printing temperature was set at 150 °C, the layer thickness at 0.2 mm, the print speed at 10 mm/s and the building plate was heated at 40 °C.

2.2.11. Dissolution test

An Eppendorf ThermoMixer® C (Eppendorf AG, Germany) was used to perform the dissolution tests with the filaments. The temperature was set at 37 °C and the rotation speed at 600 RPM. The filaments were placed in 2 ml Eppendorf® and filled with 1.5 ml of dissolution medium that was consisted of 2 % (w/w) Polysorbate 20® in 0.001 N HCl as adapted from the guidance published by the Food and Drug Administration (Dissolution Database for PP) (Dissolution Methods Database, 2021). For the 3D printed implants, the dissolution test was performed in a GFL® (Burgwedel, Germany) water bath kept at 37 °C. Implants were placed in 20 ml of dissolution medium. The *in vitro* dissolution studies were performed in triplicate over 90 days on filaments and implants. To preserve sink conditions, the dissolution medium was completely changed at each sampling time.

3. Results and discussion

3.1. Characterization of raw materials

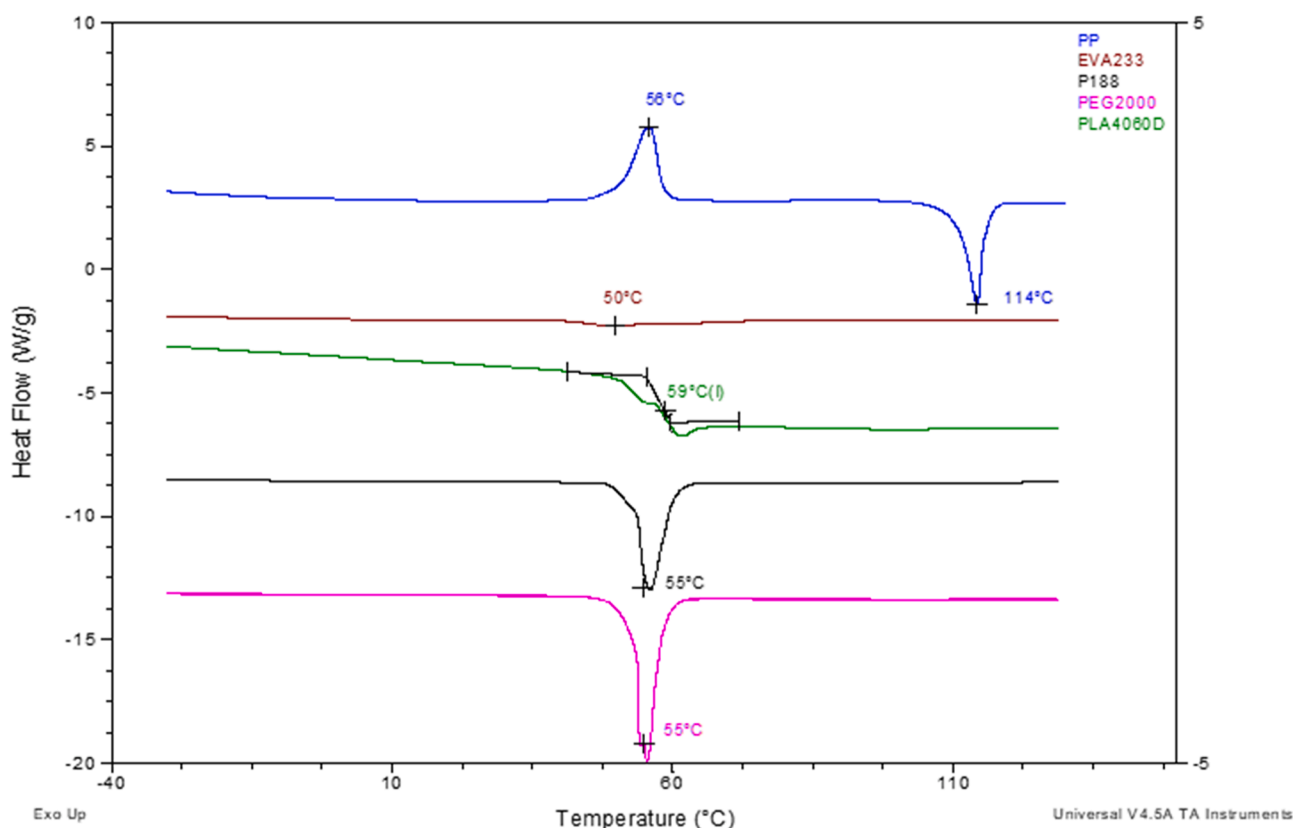Along the successive steps to get a final printable dosage form,

Fig. 2. DSC analysis of the different starting materials on the 2nd heating (heating rate: 10 °C/min).

multiple heating processes are often required and may have an adverse structural effect on API and its associated materials. For that reason, thermal analyses on starting materials were conducted to better understand the thermal stability of our different constituents during the HME and 3D printing processes. Thermal transitions of the different materials were first studied by DSC analyses.

The DSC curves corresponded to the results obtained from the 2nd heating cycle (Fig. 2). Indeed, a heating and a cooling ramp were applied to the different starting materials to eliminate their thermal history. The results showed that after a first heat/cool cycle, PP crystallized upon the second heating cycle with a cold crystallization peak at 56 °C and a melting point at 114 °C. EVA showed a wide melting range with a maximum at 50 °C. For PLA4060D, only one single T_g was identified on the 2nd cycle at 59 °C, in agreement with its amorphicity and in correlation with the literature (Ruellan et al., 2015). PEG2000 and P188 presented a similar melting point at 55 °C.

Then, a TGA was carried out on the different starting materials providing initial information about their thermal stability. This analysis provided the maximum values that should not be exceeded during thermal processes to avoid any thermomechanical degradation (e.g. HME or 3D printing).

The results obtained from the percentage weight loss and the first derivative of the different constituents, PLA, P188 and PEG, did not show any mass loss before 300 °C (Fig. 3). On the other hand, PP presented a lower thermal stability than the polymers as its weight loss started at 200 °C. Indeed, a degradation step from PP could be observed between 200 °C and 300 °C, confirmed by its first derivative with a maximum peak at 300 °C. In this case, 200 °C was determined as the maximum temperature that should not be exceeded during our various thermal processes. In addition, none of the starting materials contained any residual moisture. However, TGA did not provide any chemical data about PP and its potential chemical degradation throughout the manufacturing processes. Indeed, other chemical processes might

happen during the different processes, which may chemically induce the API degradation. Working at a temperature lower than 200 °C might be insufficient to avoid any potential chemical instabilities or degradation of PP. For that reason, a liquid–liquid extraction followed by an HPLC-UV analysis was carried out after these thermal processes to evaluate the chemical integrity of the drug (see filaments and implant preparation). In order to evaluate the crystalline structure of PP as well as of the polymers before HME and FDM, XRD analysis were also made on these raw materials (Fig. 4).

The XRD results of the different products showed that neither PLA4060D or EVA233 presented any diffraction peaks. Poloxamer® 188 showed two characteristic peaks at 19° and between 22° and 23° (Xie et al., 2009). On the other hand; PEG 2000 showed four diffraction peaks at 13.5°, 19.1°, 23.2° and 27.2° (Xiang et al., 2013). Two major peaks; at 5.1° and 7.7°, were observed for PP, corresponding to its crystalline structure (Leng et al., 2014). In comparison to other excipients diffractograms; PP was the only element presenting two major peaks
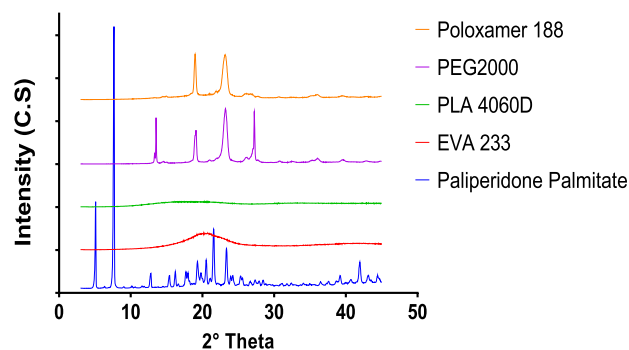
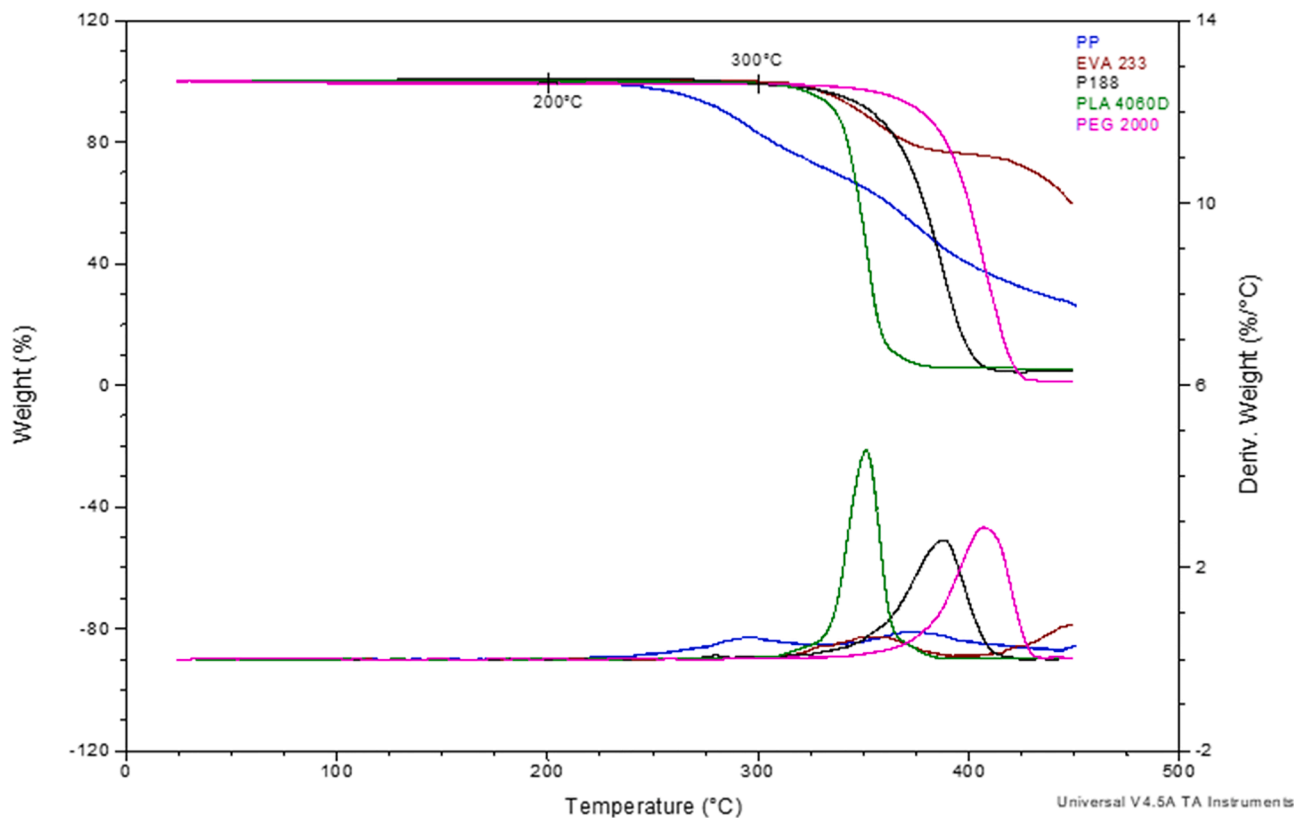**Fig. 4.** XRD analysis of raw materials.

Fig. 3. TGA analysis of starting materials presented as weight loss (%) (UP) and its first derivative (DOWN) with a heating rate of 10 °C/min under nitrogen gas (flow rate: 60 ml/min).

between 3° and 10°. Based on that, these two peaks were used in the following part to highlight the presence of crystals PP residues in blends.

3.2. Preformulation blends

Nevertheless, HME and 3D printing by FDM brought enough thermal stresses to the various components of the formulations. According to the TGA results (Fig. 3), 200 °C was the maximum temperature that PP could withstand. This temperature was closer to the usual processing temperature of PLA, which is usually ranged between 180 °C and 200 °C (Boetker et al., 2016; Jamróz et al., 2018). Moreover, other parameters such as, shear, the screw design, the pressure and the residence time in the extruder may induce some degradation to API (Huang et al., 2017).

In order to decrease the processing PLA temperature, different types of plasticizers were often used. Plasticizers are available in liquid or solid form. However, liquid plasticizers, such as citrate esters or tri-acetin, do not allow homogeneous mixing with powder constituents. In addition, evaporation or demixing of liquid plasticizers may lead to some stability issues in the final product (Desai et al., 2018). In this work, the use of solid plasticizers was selected as an adequate solution. Indeed, both PEG 2000 and Poloxamer 188 were selected for their plasticizing effect and their current use in HME (Desai et al., 2018; Zhang et al., 2014; Yu et al., 2015; Lauer et al., 2018). On the other hand, EVA was selected for its hydrophobicity, low processing temperature and its suitability for the preparation of subcutaneous implantable dosage forms, especially by HME (Schneider et al., 2017). The pre-formulation blends, consisting of PLA_PEG, PLA_P188 and PLA_EVA mixtures (Table 1), were prepared by HME. The process involved to blend the mixtures at 180 °C for 5 min using a Brabender® extruder. Then, the mixtures were cooled, grounded into a fine powder and sieved through a 40mesh sieve to remove any large agglomerates. Then, an extrusion test at a temperature slightly above the melting temperature of PP was conducted on the different blends. The selected temperature was 125 °C, which was 10 °C above the melting temperature of PP. Working at a temperature slightly above the melting point of PP prevented the screws from blocking during the HME process. All formulations were finally evaluated by DSC to determine whether the excipients had an impact on the Tg of PLA.

On the first heating cycle, the DSC results showed a decreased of the Tg to 43 °C, 38 °C and 54 °C for the PLA_P188, PLA_PEG and PLA_EVA mixtures, respectively (Fig. 5). The analysis was performed on the first heating cycle to obtain the T_g of the different formulations just after their preparation. Indeed, the characteristics seen in the first heating correspond to the state of the samples after extrusion without any further cooling or heating applied during the DSC analysis. Both P188 and PEG 2000 had a clear plasticizing effect on PLA4060D, decreasing the T_g of the polymer by 16 °C and 21 °C, respectively. On the other hand, EVA did not clearly affect the T_g of PLA4060D. Indeed, the presence of 20 % w/w of EVA only decreased the T_g by 5 °C. While 10 % w/w of PEG or P188 decreased the Tg of PLA4060D, respectively by 36 or 27 %. Despite this, all blends have been successfully extruded at 125 °C without blocking the screws. In the case of PLA_EVA, the low melting temperature of EVA (55 °C) and its presence at 20 % w/w in the mixture resulted in a lower extrusion temperature compared to PLA4060D without additives. Then, the pre-formulations were ground by cryogenic milling and sieved to obtain a fine powder.

Table 1
Different blends processed with the Brabender© – Temperature set at 180 °C and the rotation speed kept at 150 RPM for 5 min.

Formulations	PLA (%) w/w	EVA (%) w/w	P188 (%) w/w	PEG (%) w/w
PLA_P188	90	–	10	–
PLA_PEG	90	–	–	10
PLA_EVA	80	20	–	–

3.3. Filaments and implants preparation

Subsequently, PP was added to the various pre-formulations to achieve the described drug-loaded formulations (Table 2). After the addition of the drug, cryogenic milling was applied on the freshly prepared drug-loaded formulations. This milling step allowed the preparation of an homogeneous and intimate mixture of our different constituents (Allaf et al., 2019). After the milling step, the preparation of printable filaments from the mixtures was carried out. Through the HME process, the feeder, the screws and the winding speed were adjusted to control the filament diameter. The obtained filaments were characterized by a diameter of 1.75 ± 0.1 mm which was suitable for the Hyrel® 3D printer. Then, the different filaments were analyzed by DSC and XRD. In order to assess the integrity of the drug after its thermal process, PP was extracted using a liquid–liquid extraction technique and quantified by a HPLC-UV method. Both the amount and integrity of PP were evaluated accordingly.

First, DSC analysis was performed on the different extruded filaments to highlight the different thermal transitions as well as the impact of PP on the pre-formulations blend (Fig. 6).

The DSC result showed different thermal transitions in the obtained filaments right after their preparation, during the first heating cycle. A decrease of the T_g was observed for PLA_P188_PP and PLA_PEG_PP mixtures. The observed values were 35 °C and 32 °C respectively for PLA_P188_PP and PLA_PEG_PP, compared to 43 °C and 38 °C in blends without PP.

For PLA_EVA_PP, the DSC results showed a T_g at 52 °C, slightly lower than that obtained without PP. Moreover, the plasticizing effect of PEG and P188 on PLA4060D, an additional decrease of the T_g was observed. The presence of 10 % w/w of PP allowed a slight additional decrease of T_g observed in all blends. Indeed, the impact of a drug acting as a plasticizer has been observed in other drug-polymer blends in the literature (de Brabander et al., 2002; Islam et al., 2015).

In addition to the T_g, cold crystallization peaks corresponding to PP were also observed at 62, 64 and 80 °C for PLA_P188_PP, PLA_PEG_PP and PLA_EVA_PP, respectively. These cold crystallization peaks appeared at higher temperatures than that for amorphous PP, which was of 56 °C (Fig. 2). The impact on the minimum temperature required to crystallize PP was related to the formulations. Indeed, the highest value was observed for PLA_EVA_PP with an increase of 24 °C. On the other hand, a relatively low increase was noticed for the formulations based on PLA_P188 and PLA_PEG. In their work, *Sarpal et al*, prepared amorphous solid dispersion based on melt-quenched drug-loaded polymers. They observed an increase in the cold crystallization peak by DSC, which was correlated as an indicator of the strength of drug-polymer interaction (Sarpal et al., 2019). These observations were also shared by *Bhugra et al.* who worked on the physical stability drug-loaded polymers system. They observed that higher cold crystallization temperatures were related to longer stability overtime (Bhugra et al., 2016).

Finally, the melting point of PP in the different blends was observed at 106, 107 and 104 °C for PLA_P188_PP, PLA_PEG_PP and PLA_EVA_PP, respectively. This melting point appeared to be 10 °C lower than that from pure PP. A decrease of the melting point of a drug might be due to the miscibility of this drug in the blend. On the other hand, immiscible or partially miscible drug-polymer system would not show any melting point decrease (Marsac et al., 2009). In this case, the endotherm of PP was related to amorphous drug-rich nanodomains as the event was taking place right after a cold crystallization peak. Indeed, *Sarpal et al.* reported this phenomenon and suggested amorphous drug-rich domains can rearrange into crystalline phases correlated to an increased mobility of the system above Tg (Sarpal et al., 2019).

In order to complete these observations, XRD analysis was carried out throughout the various preparation steps of the printable filaments. Indeed, the samples were analyzed before and after cryogenic milling, as well as after the extrusion of the filaments. This analysis highlighted the impact of these different processes on the PP state. Both cryogenic
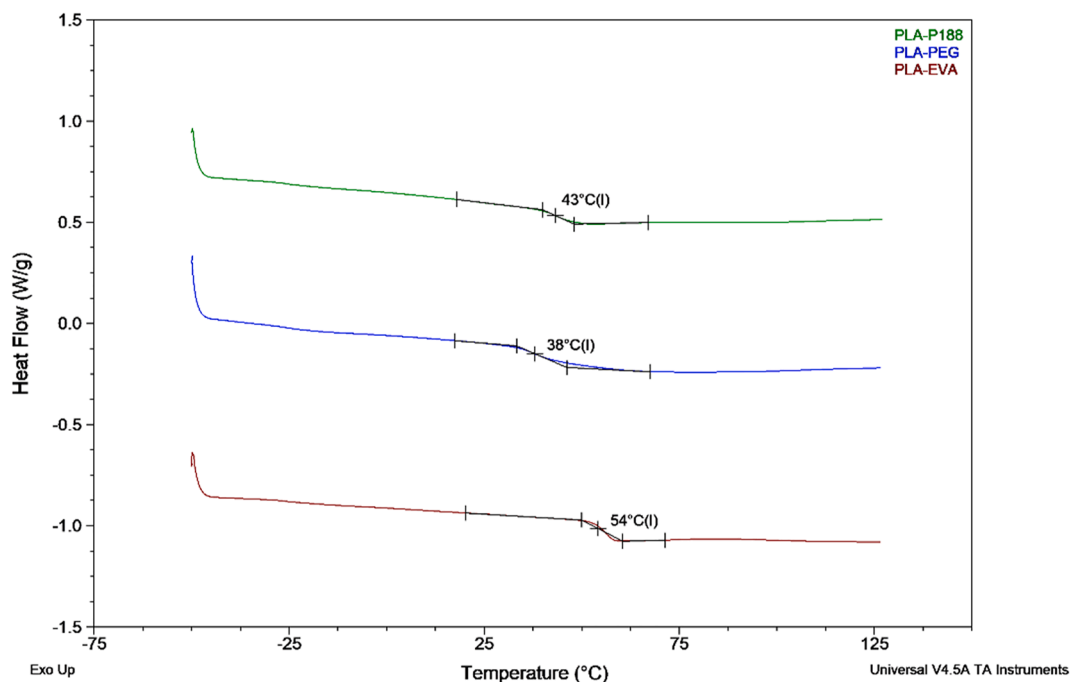
Fig. 5. DSC analysis of preformulation analysis on the 1st heating cycle (heating rate: 10 °C/min).

Table 2
Composition of the different formulations.

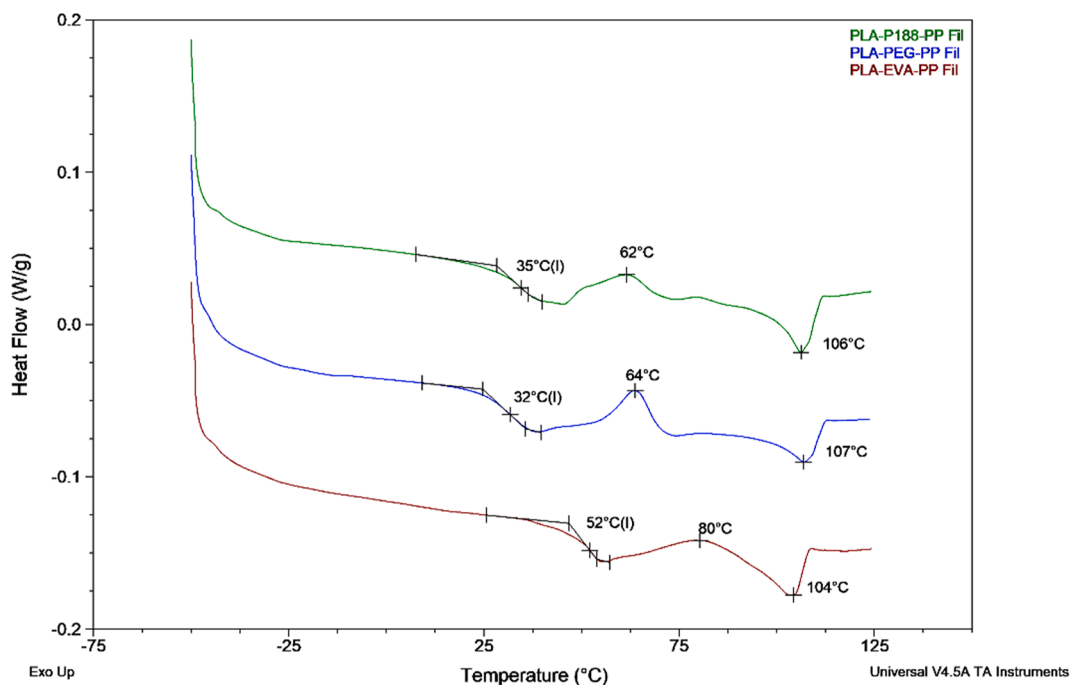| Formulations	PLA (% w/w)	EVA (% w/w)	P188 (% w/w)	PEG (% w/w)	Theoretical loading of PP (% w/w)	Experimental PP (% w/w) (mean ± SD, n = 3)
PLA_PEG_PP	81	–	–	9	10	9.6 ± 0.1
PLA_P188_PP	81	–	9	–	10	9.8 ± 0.1
PLA_EVA_PP	72	18	–	–	10	9.8 ± 0.3

Fig. 6. DSC analysis of the filaments after HME process: PLA_P188_PP, PLA_PEG_PP and PLA_EVA_PP (first heating cycle, heating rate: 10 °C/min).
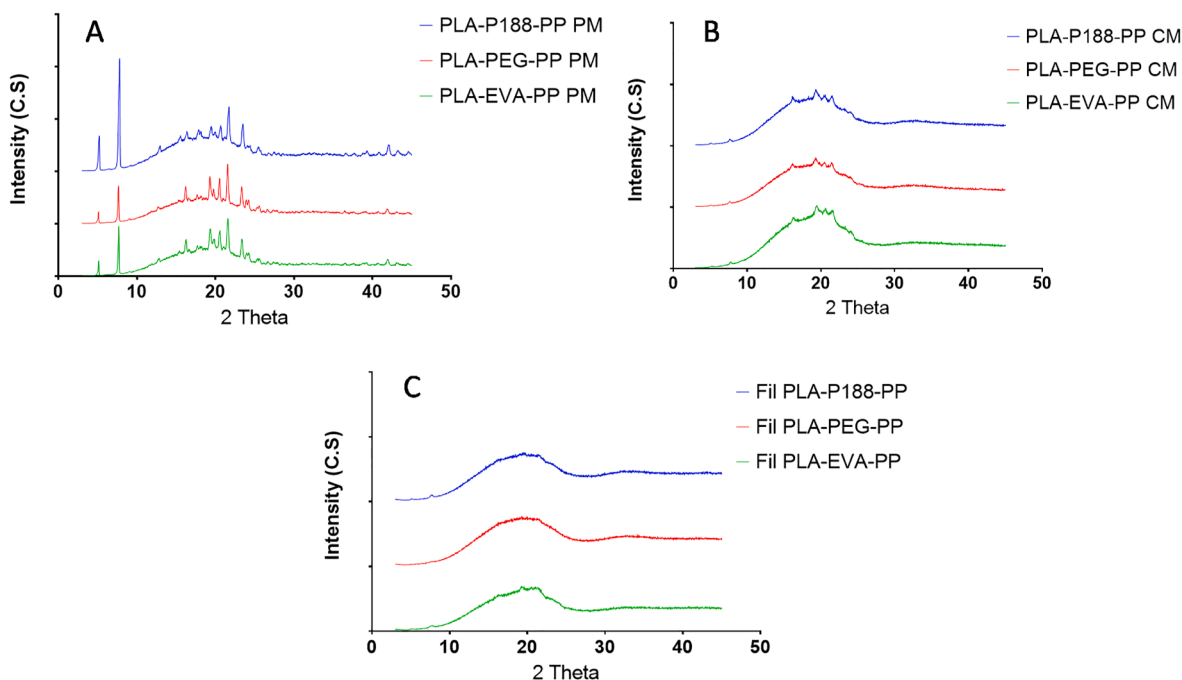
Fig. 7. XRD analysis on the formulations before (A), after cryogenic milling (B) and after HME process (C).

milling and HME process involved the application of mechanical and/or thermal energy to the various constituents of the blends.

Investigating the physical mixtures of PLA_P188_PP, PLA_PEG_PP and PLA_EVA_PP, before the cryogenic milling (Fig. 7A), showed the different diffraction peaks of crystalline PP. Indeed, both characteristic peaks between 3° and 10°, at 5.1° and 7.7° from PP can be clearly highlighted regardless the formulation. In Fig. 7B, i.e., after the cryogenic milling stage, a clear decrease in the intensity of PP diffraction peaks was observed. Indeed, due to the mechanical stress involved during the milling step, it allowed an intimate mixing of the different constituents and a partial amorphization of the drug. Milling crystalline materials may lead to their amorphization by disrupting the crystalline lattice. However, the material is subjected to high energy milling and so, significant heat that may induce some thermal degradation. Through the use of cryogenic milling, under liquid nitrogen, the excess of heat produced during the milling stage could be avoided (Moinuddin et al., 2017; Manini et al., 2021).

On the other hand, after the final extrusion stage (Fig. 7C), no diffraction peaks of PP were observed in the filaments, corresponding to its amorphous state which was in correlation to the DSC results. The thermal process, the shear force applied by the screws and the rapid cooling of the filament after extrusion completed up the amorphization of PP. However, the chemical degradation that may occur during cryogenic milling or HME process could not be merely assessed by DSC or XRD analyses. Therefore, the integrity and the quantification of PP was evaluated after a liquid–liquid extraction, from the extruded filaments at the end of the process (Table 2).

After our different processes, the percentages of PP after extraction from the filament in the different formulations were 9.6 ± 0.1 %, 9.8 ± 0.1 % and 9.8 ± 0.3 % from PLA_P188_PP, PLA_PEG_PP and PLA_E-VA_PP%, respectively. In addition, no evidence of PP degradation was observed through these analyses. Based on these values, it could be concluded that the chemical stability PP was preserved through the different milling and extrusion stages.

However, before being printed, a first screening was performed on the different formulations. An *in vitro* dissolution test was carried out on different samples obtained from PLA_P188_PP, PLA_PEG_PP and PLA_EVA_PP filaments (Fig. 8). The motivation of this test was to assess the release of PP after 90 days from the different formulations. For this
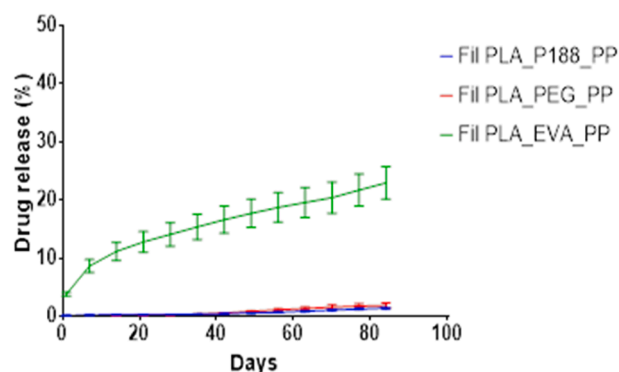

Fig. 8. Cumulative percentage of PP released overtime from filaments based on PLA_P188_PP, PLA_PEG_PP and PLA_EVA_PP (mean ± SD, n = 3).

purpose, different samples of the formulations were placed in 2 ml Eppendorf© and filled with 1.5 ml of dissolution medium. During the *in vitro* dissolution test, the medium was replaced at each sampling time and analyzed by HPLC-UV to quantify the amount of PP released.

After 1 day of dissolution, no PP was released from the filaments based on PLA_P188_PP and PLA_PEG_PP formulations. On the other hand, 3.8 ± 0.3 % of PP was released after 1 day of dissolution from the PLA_EVA_PP formulation. Then, after 90 days of dissolution, only the PLA_EVA_PP based formulation showed a continuous and sustain release of PP with time to reach 22.9 ± 2.8 % after 90 days. In contrast, both PLA_P188_PP and PLA_PEG_PP released less than 2 % PP after 90 days. These results were in correlation with those obtained by *Li et al.* In their study, they investigated different ratios of dexamethasone loaded PLA-poloxamer blends prepared by HME. The drug release was studied through an *in vitro* dissolution test and the samples were placed in a 0.1 M phosphate buffered saline with 0.5 % v/v of Tween®80. They observed that formulations based on PLA-F68 90–10 (w/w), loaded with 10 or 25 % w/w of dexamethasone, did not release more than 2.5 % w/w of API after 120 days of dissolution test (Li et al., 2013). As a filament is a semi-finished product, the following part on 3D printing was carried out with the PLA_EVA_PP formulation which allowed a sustained release of
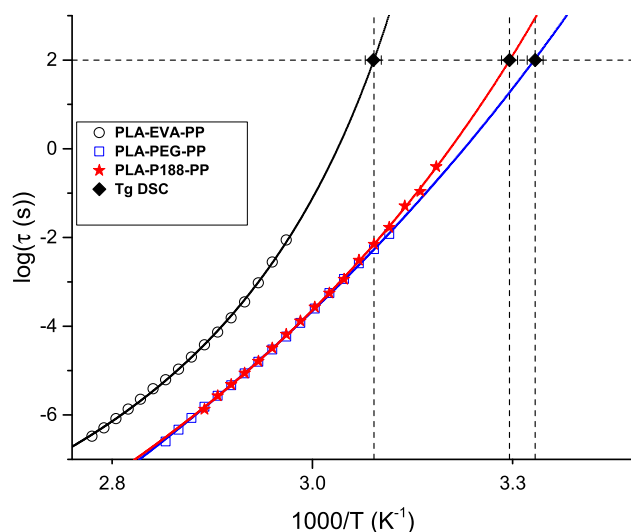
Fig. 9. Relaxation time of PLA_EVA_PP, PLA_PEG_PP and PLA_P188_PP filaments as a function of temperature.

the drug overtime.

To complete these observations, dielectric spectroscopy was used to characterize the molecular mobility of the different formulations studied in the *in vitro* dissolution test on filaments (Fig. 9). Indeed, the polymer type and in this case the pre-formulation blend might have an impact on the molecular mobility within the filament. BDS is then an interesting technique to monitor the molecular mobility as it displayed in relaxation processes over a wide range of frequency and at different temperatures (Grzybowska et al., 2016).

Based on the temperature dependence of the segmental time within the interval from 30 to 85 °C, PLA_EVA_PP showed a clear lower molecular mobility than PLA_P188_PP and PLA_PEG_PP. In addition, the extrapolated T_g from BDS evaluation (Table 3) were in agreement with those observed by DSC (Fig. 6).

As already mentioned, at a temperature higher than T_g, an increase of the molecular mobility may enhance the crystallization ability (Wang et al., 2021) of the drug, and reduces the temperature at which cold crystallization takes place. Indeed, DSC measurements showed that the crystallization peak of PP appeared at a higher temperature for the filament based on PLA_EVA_PP mixture compared to the other formulations. This result can be easily explained considering that, as the molecular mobility got reduced, it took a longer period of time for PP to crystallize. On the other hand, the PLA_P188_PP and PLA_PEG_PP formulations showed a T_g being roughly 20 °C lower than PLA_EVA_PP, indicating an enhanced molecular mobility. During the *in vitro* dissolution test, the filaments were placed at 37 °C for 3 months. Such temperature was higher than the T_g of PLA_PEG_PP and PLA_P188_PP, which allowed a faster crystallization of PP and a significant reduction of its release from the corresponding filaments.

After this screening test, the filament based on the PLA_EVA_PP was selected and printed as an implant using the Hyrel® 30 M 3D printer equipped with a MK-1 head. During the printing, the temperature was set at 150 °C, the printing speed at 10 mm/s and the heating plate at 40 °C to ensure a good adhesion between the printed layer and the building plate. The shape of the implant has been designed via

Table 3
Comparison of Tg obtained by BDS and DSC.

Sample names	T_g (BDS) (°C)	T_g (DSC) (°C)
PLA-EVA-PP	53 ± 1	52
PLA-PEG-PP	32 ± 1	32
PLA-P188-PP	35 ± 1	35

Tinkercad© (Fig. 10, A).

On the market, subcutaneous implants are shaped as long cylinders. For instance, Viadur™ leuprolide acetate-loaded implant is designed as a reservoir-based system characterized by a diameter of 4 mm and a length of 45 mm (Simpson et al., 2020). Norplant™ is a contraceptive system that is loaded with levonorgestrel and measures 2.4 mm in diameter and 4.4 cm in length (Kleiner et al., 2014). Lastly, Supprelin™ and Vantas™ are both subcutaneous implants based on histrelin acetate, characterized with a diameter of 3 mm and 3.5 cm in length (Simpson et al., 2020).

3D printing is a highly versatile technology, allowing the conception of complex structure. In addition to the overall implant design, specific parameters applied in 3D printing may impact the surface of the final dosage form. In this work, a slightly flattened shape was designed to allow the modulation and evaluate the influence of the infill percentage on the release profile of the 3D printed implant. Indeed, a monolithic shape could be obtained with an infill of 100 % while an infill equal to 0 % corresponds to a hollow shape. The parameters that were selected to design our implants were 100 % of infill (Fig. 10, B left) and 20 % of infill (Fig. 10, B right). All implants were printed with a layer thickness of 200 μm. Following the 3D printing, the surface area and volume of the implants were determined using the Meshmixer© software (Table 4).

When the printed device did not present any bottom or top layers, the infill percentage has a direct impact on the surface area and the volume of the final dosage form. In this case, decreasing the infill from 100 %, corresponding to a monolith, to 20 % increased the surface area of the implant. Indeed, the theoretical surface of the monolith which was evaluated with Meshmixer© was found to be 316.1 mm^2 and increased to 474.2 mm^2 when the infill was fixed at 20 %. Nevertheless, decreasing the infill of the device also decreased its volume. Indeed, the volume of the implant decreased from 281.2 mm^3 for a 100 % of infill to 188.7 mm^3 for a 20 % of infill. In addition, the surface-to-volume ratio of the implants was higher when an infill of 20 % was set, compared that of the monolith.

The experimental values obtained with the 3D printed implants showed a surface area of 491.9 ± 18.9 mm^2 & 314.1 ± 8.7 mm^2 for the infill 20 and 100 %, respectively. The obtained volume for the 20 and 100 % implants were 200.1 ± 11.7 mm^3 and 312.6 ± 16.8 mm^3. The overall surface-to-volume ratio was maintained with a 2.5 ± 0.1 & 1 ± 0.1 mm^2/mm^3 ratio.

Even if the experimental volume of the monolith was 10 % higher than expected, this value could be attributed to some slight differences in the 3D printing process. However, all the other values were within the standard deviations and the overall S/V ratio was preserved. The weights of the implants were of 157.9 ± 6.2 mg and 364.7 ± 14.7 mg for 20 and 100 % of infill, respectively.

Individual implant was placed in glass flasks which were filled with 20 ml of a similar dissolution medium than that used for our screening tests. The flasks were placed in an GFL bath, heated at 37 °C with an orbital agitation of 50RPM for 90 days for the *in vitro* dissolution test. After each sampling time, the dissolution medium was replaced. The amount of PP that was released with time was quantified by an HPLC-UV method. The cumulative percentage of PP that was released from the implants with an infill of 20 and 100 % as well as the obtained results of the filament are represented in Fig. 11. In addition, GPC analysis was conducted on the PLA_EVA_PP filaments, on the 3D printed implants after 90 days *of in vitro* dissolution test.

After 1 day of *in vitro* dissolution test, the implants with 100 % of infill released 2.5 ± 0.3 % of PP. On the other hand, the implant with an infill of 20 % showed a higher release of PP which reached 6.3 ± 0.5 % after 1 day. The implant with the largest surface area had the highest initial release percentage, in opposition with the monolith implant. At the end of the 3-month *in vitro* dissolution test, the implants based on 20 and 100 % infill released 15.0 ± 0.8 % and 5.6 ± 0.6 % of PP, respectively. Therefore, the percentage of release was 2.7 times higher for the implants with a 20 % infill compared to the monolith. In comparison, the
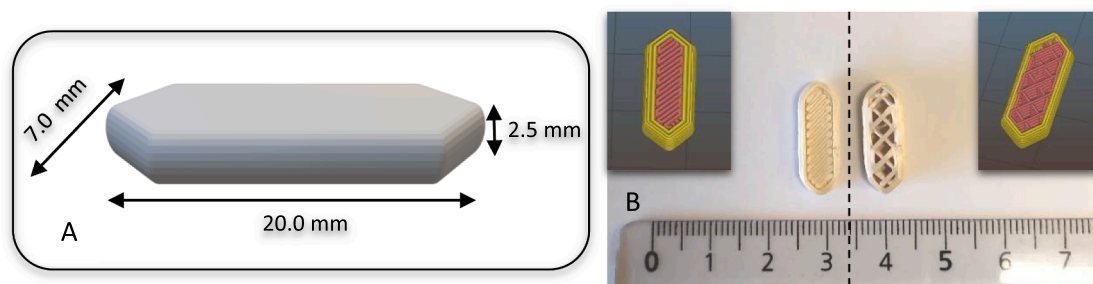
Fig. 10. Dimensions of the final implant (A), 3D printed implants (B).

Table 4
Table representing the theoretical and experimental surface (mm^2), volume (mm^3) and surface/volume ratio (mm^2/mm^3) of the 3D implants.

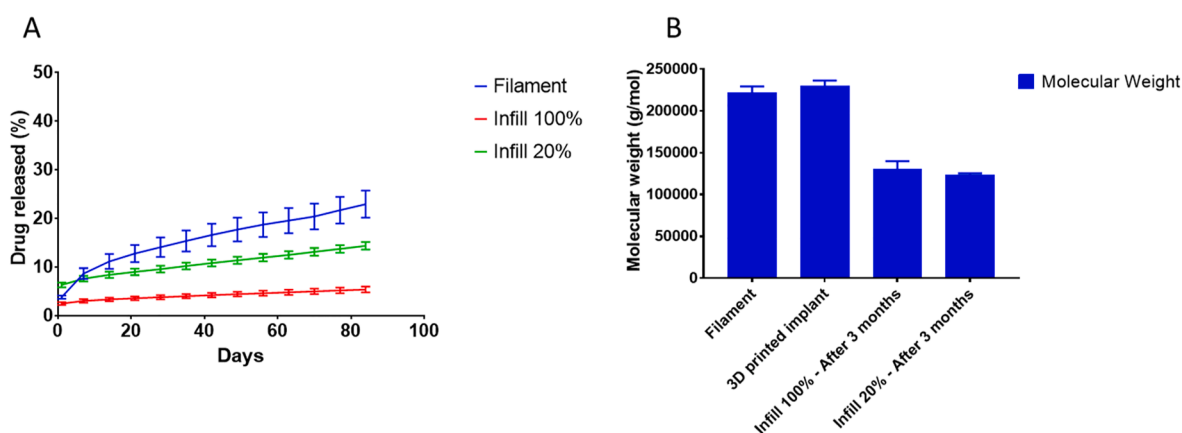| Infill (%)	Theoretical values			Experimental values (mean ± SD, n = 3)			
	Surface (mm^2)	Volume (mm^3)	S/V (mm^2/mm^3)	Surface ± SD (mm^2)	Volume ± SD (mm^3)	S/V (mm^2/mm^3)	Weight (mg)
20	474.2	188.7	2.5	491.9 ± 18.9	200.1 ± 11.7	2.5 ± 0.1	157.9 ± 6.2
100	316.1	281.2	1.1	314.1 ± 8.7	312.6 ± 16.8	1 ± 0.1	364.7 ± 14.7

Fig. 11. A) Cumulative percentage of PP released overtime from PLA_EVA_PP formulation (mean ± SD, n = 3). B) Molecular weight (g/mol) of Filament, 3D printed implants and implants (100 % and 20 % infill) after 90 days based on PLA_EVA_PP (mean ± SD, n = 3).

filaments based on PLA_EVA_PP released 3.8 ± 0.3 % of PP after 1 day and 22.9 ± 2.8 % of PP after 90 days of dissolution test. In addition, based on GPC results (Fig. 11, B), no degradation of the polymer was observed after the 3D printing process at 150 °C in the presence of the drug. The slight differences in mass loss between the filament and the 3D printed implants were within the standard deviations. This is an important point because the presence of tertiary amine in the PP can be the starting point of amine-catalyzed hydrolysis and a faster degradation of PLA. Indeed, it has often been reported that risperidone in the presence of PLGA can accelerate the degradation rate of the polyester by the presence of amine associated with its piperidine ring (Kohno et al., 2020; Rawat et al., 2011; Shen et al., 2016). In this study, neither HME or the 3D printing step caused a polymer matrix degradation. However, the presence of the piperidine ring in PP might increase the degradation rate of PLA during the dissolution test. Indeed, after 90 days of *in vitro* dissolution test, a clear mass loss was observed for both implants. Independently of the infill, the 3D printed implants presented an average mass loss of 45 ± 1 % w/w. The decrease in M$_w$ is explained by the degradation rate of the polymer succeeding the penetration of dissolution medium into the dosage form. The degradation of the polymer matrix is due to the hydrolytic cleavage of its ester linkages leading to the surface and bulk erosion of the 3D printed implant (Bode et al., 2019). The differences of drug release could be thereby explained by the surface-to-volume ratio of the different implants. In fact, the

implant with the infill of 20 % showed a S/V ratio of 2.5 compared to 1.0 for the monolith. In comparison, the filaments used for the screening test presented a theoretical surface and volume of 36.4 mm^2 & 13.4 mm^3, respectively. These values corresponded to a surface-to-volume ratio of 2.7 mm^2/mm^3, which was still higher than that of the 20 % infill implant. *Khaled et al.* worked on the geometry of the 3D printed acetaminophen-loaded tablets and showed that the surface area and the geometry had in impact on the drug release profile. They observed that the drug release from the 3D printed tablets was correlated to the S/V ratios, the higher the ratio was, the faster the drug released (Khaled et al., 2018). Therefore, the dissolution profile of PP obtained from the filament could be explained by its cylinder shape which allowed a higher S/V ratio than the 20 % and 100 % of infills. However, the results observed for the filament and the 20 % infill implant showed a constant and sustained release of PP over 3 months in this study.

Nevertheless, these results showed that different and tailored released profiles might be obtained from a single formulation. In this case, no change has been made to the formulation, by only modulating the geometry of the final dosage form into different release profiles. Further studies with different infill range and geometries should be investigated, especially the impact on the surface area, the volume and their S/V ratio. A prediction system could be interesting to determine the ideal implant design for each patient's specific need. New technologies, such as artificial intelligence can be applied to predict the

printability and drug release from FDM-based systems (Elbadawi et al., 2020). *Muñiz Castro et al.*, employed a machine learning approach over a large number of formulations to predict the different drug dissolution profiles (Muñiz Castro et al., 2021). However, *in vivo* studies are essential to complete the above observations. Indeed, *Li et al.* compared the drug release from implantable devices made of drug-loaded PLA that did not release more than 2.5 % of drug over 4 months *in vitro*. The same implants released up to 20 % of drug within 30 days *in vivo*. It may be observed that *in vitro* dissolution test, or the latest particle-oriented dissolution method, cannot encompass the complexity observed *in vivo*, especially for long-acting implants (Darville et al., 2014; Bhardwaj and Burgess, 2010).

3.4. Stability

Stability evaluations provide interesting information on how the quality of a drug varies with time under different conditions. In order to test the stability of PLA_EVA_PP formulation that was used in this study, 3D printed implants were prepared. The 3D printed dosage forms were placed in vials, flushed with nitrogen and sealed. Due to the presence of a polymer matrix, the implants must be stored at a low temperature (Andhariya et al., 2019). For that reason, the vials were placed at 25 °C and at 4 °C.

XRD, drug extraction and GPC analysis were assessed during this stability study. XRD analysis was performed on 3D printed implants to assess the stability of the amorphous form of PP as a function of the storage and temperature. On the other hand, GPC analysis was performed after 3 months to investigate the stability of the polymer at 25 °C and 4 °C.

The results presented on Fig. 12A and B showed the XRD analysis obtained during the stability evaluations. Fig. 12A represented the XRD results from 3D printed dosage forms stored at 4 °C after 1, 2 and 3 months of storage. An amorphous halo shape was observed at the different time and no crystal residue of PP was observed. Fig. 12B

showed the results obtained at a temperature of 25 °C after 1, 2 and 3 months. The diffractograms did not show the presence of PP diffraction peaks, which correspond to crystals residues. The amorphous form of PP obtained after the different processes (mechanical and/or thermal) was maintained for at least 3 months at 4 °C and 25 °C. These observations were in correlation to those obtained by DSC and BDS (Table 3) as the storage temperatures were lower than the T_g of the PLA_EVA_PP formulation.

GPC evaluation allowed comparing the Mw of filaments that were freshly prepared and that of the implants after a storage of 3 months at 25 °C and 4 °C (Fig. 12C). The results did not show any differences in mass loss between the samples, regardless of the storage temperature. In addition, the stability of PP in the 3D implants was assessed after 3 months. PP was extracted and quantified after being stored at 25 °C and 4 °C. The results showed a mean recovery of 97.3 ± 1.3 % and 96.9 ± 1.4 % after 3 months of storage, respectively at 4 °C and 25 °C. The stability of the drug was preserved, and no degradation were observed. These results agreed with an appropriate stability of 3D printed drug-loaded implants stored for 3 months at 4 °C and 25 °C.

4. Conclusion

In this work, the printability of PP in different matrices was considered. The use of solid plasticizers such as PEG2000 or P188 allowed decreasing the process temperature of the formulation but not a sustain drug release. However, the use of a polymer with a low processing temperature, such as EVA, allowed decreasing the processing temperature and obtaining a constant release of PP. The use of 3D printing has shown the possibility to modulate the design of the final implantable form. Nevertheless, the results obtained highlighted the importance of crucial parameters such as the surface area or the S/V ratio and the fact they must be determined in advance for the patient's needs. Stability tests carried out on implantable forms stored at 25 °C and 4 °C for periods of 1, 2 and 3 months, showed the stability of the
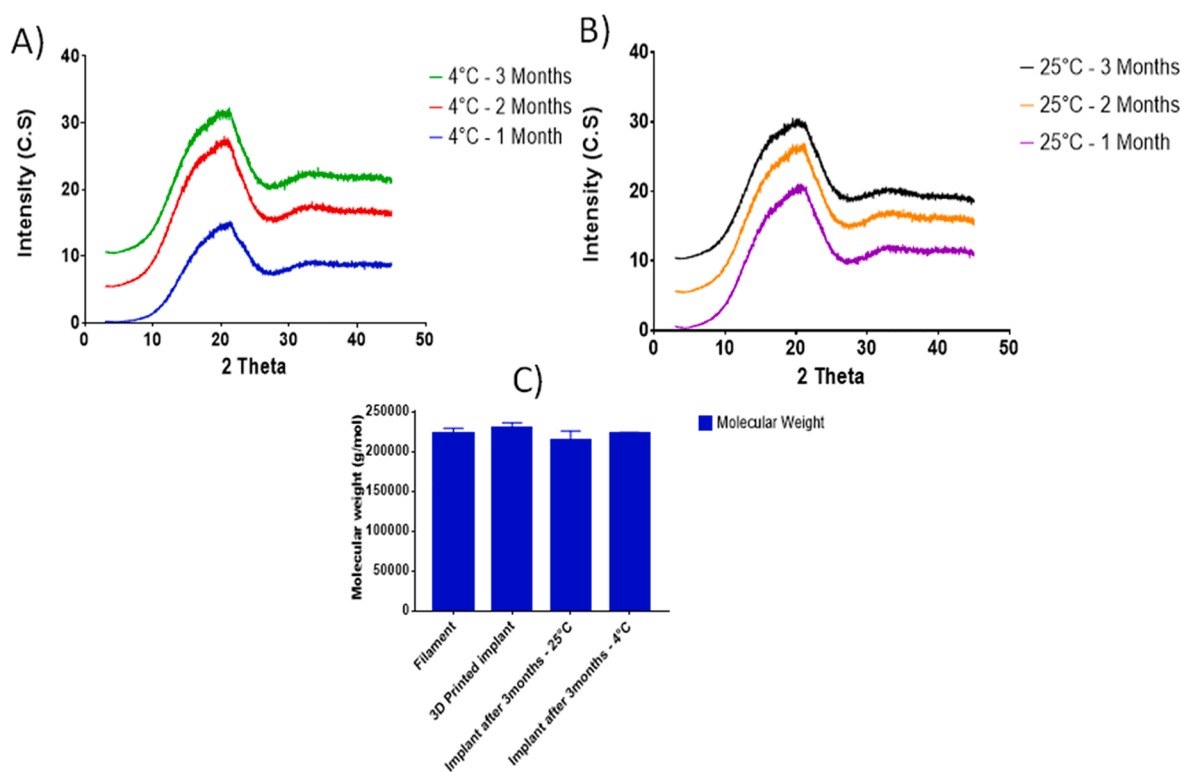

Fig. 12. XRD stability test on 3D printed PLA_EVA_PP based formulation on time and storage temperature A) stored at 4 °C; B) stored at 25 °C; C) GPC analysis of implants after 3 months stored at 25 °C and 4 °C (mean ± SD, n = 3).

amorphous form of PP over time by XRD. However, given the small amount of PP present in the implantable form, other techniques as dynamic vapor sorption, should be considered to evaluate the amount of amorphous PP. Similarly, a kinetic study of the crystallization of PP would provide more information on the stability of the drug in the body and at different storage temperatures. Finally, these results showed that it is possible to modulate the design of an implantable form using 3D printing. Different release profiles can be obtained and adapted to the specific needs of each patient from a single formulation. However, a predicting system allowing the determination of the amount of drug released over time as a function of design would provide a better understanding of the release kinetic. Nevertheless, this concept of tailored dosage form and sustain drug release could be adapted to other drugs and diseases. Indeed, a polymer matrix with a high T_g in addition to its low processing temperature and adaptability for 3D printing is an asset for the creation of long-acting tailored dosage forms and personalized medicine.

CRediT authorship contribution statement

Giuseppe Manini: Investigation, Formal analysis, Writing – original draft. **Samira Benali:** Writing – review & editing. **Allen Mathew:** Formal analysis. **Simone Napolitano:** Validation, Writing – review & editing. **Jean-Marie Raquez:** Supervision, Validation, Writing – review & editing. **Jonathan Goole:** Supervision, Validation, Writing – review & editing.

Declaration of Competing Interest

The authors declare that they have no known competing financial interests or personal relationships that could have appeared to influence the work reported in this paper.

Acknowledgements

References

Prasad, L.K., Smyth, H., 2016. 3D Printing technologies for drug delivery: a review. Drug Dev. Ind. Pharm. 42 (7), 1019–1031. https://doi.org/10.3109/03639045.2015.1120743.

Sachs E., John, H., Michael, C., Paul, W. Three-dimensional printing techniques, US Patent 5,204,055;(19).

Infanger, S., Haemmerli, A., Iliev, S., Baier, A., Stoyanov, E., Quodbach, J., August 2018. Powder bed 3D-printing of highly loaded drug delivery devices with hydroxypropyl cellulose as solid binder. Int. J. Pharm. 2019 (555), 198–206. https://doi.org/10.1016/j.ijpharm.2018.11.048.

Xu, X., Robles-Martinez, P., Madla, C.M., Joubert, F., Goyanes, A., Basit, A.W., Gaisford, S., 2020. Stereolithography (SLA) 3D printing of an antihypertensive polyprintlet: Case study of an unexpected photopolymer-drug reaction. Addit. Manuf. 33, 101071. https://doi.org/10.1016/j.addma.2020.101071.

Fina, F., Goyanes, A., Gaisford, S., Basit, A.W., 2017. Selective laser sintering (SLS) 3D printing of medicines. Int. J. Pharm. 529 (1–2), 285–293. https://doi.org/10.1016/j.ijpharm.2017.06.082.

El, A.I., Breitkreutz, J., Quodbach, J., 2020. Investigation of semi-solid formulations for 3D printing of drugs after prolonged storage to mimic real-life applications. Eur. J. Pharm. Sci. 146 (February), 105266 https://doi.org/10.1016/j.ejps.2020.105266.

Pietrzak, K., Isreb, A., Alhnan, M.A., 2015. A flexible-dose dispenser for immediate and extended release 3D printed tablets. Eur. J. Pharm. Biopharm. 96 (August), 380–387. https://doi.org/10.1016/j.ejpb.2015.07.027.

Azad, M.A., Olawuni, D., Kimbell, G., Badruddoza, A.Z.M., Hossain, M.S., Sultana, T., 2020. Polymers for Extrusion-Based 3D Printing of Pharmaceuticals: A Holistic Materials - Process Perspective. Pharmaceutics 12 (2), 124. https://doi.org/10.3390/pharmaceutics12020124.

Goyanes, A.A.A., Fina, F., Martorana, A., Sedough, D., Gaisford, S., Basit, A.W., 2017. Development of modified release 3D printed tablets (printlets) with pharmaceutical excipients using additive manufacturing. Int. J. Pharm. 527 (1–2), 21–30. https://doi.org/10.1016/j.ijpharm.2017.05.021.

Kempin, W., Franz, C., Koster, L.-C., Schneider, F., Bogdahn, M., Weitschies, W., Seidlitz, A., 2017. Assessment of different polymers and drug loads for fused deposition modeling of drug loaded implants. Eur. J. Pharm. Biopharm. 115, 84–93. https://doi.org/10.1016/j.ejpb.2017.02.014.

Jonathan, G., Karim, A., 2015. 3D printing in pharmaceutics: A new tool for designing customized drug delivery systems. Int. J. Pharm. 499 (1–2), 376–394. https://doi.org/10.1016/j.ijpharm.2015.12.071.

Feuerbach, T., Callau-Mendoza, S., Thommes, M., 2019. Development of Filaments for Fused Deposition Modeling 3D Printing with Medical Grade Poly(Lactic-Co-Glycolic Acid) Copolymers. Pharm. Dev. Technol. 24 (4), 487–493. https://doi.org/10.1080/10837450.2018.1514522.

Lim, S.H., Kathuria, H., Tan, J.J.Y., Kang, L., 2018. 3D printed drug delivery and testing systems — a passing fad or the future ? Adv. Drug Deliv. Rev. 132, 139–168. https://doi.org/10.1016/j.addr.2018.05.006.

Genina, N., Holländer, J., Jukarainen, H., Mäkilä, E., Salonen, J., Sandler, N., 2016. Ethylene vinyl acetate (EVA) as a new drug carrier for 3D printed medical drug delivery devices. Eur. J. Pharm. Sci. 90, 53–63. https://doi.org/10.1016/j.ejps.2015.11.005.

Goyanes, A., Buanz, A.B.M., Basit, A.W., Gaisford, S., 2014. Fused- filament 3D printing (3DP) for fabrication of tablets. Int. J. Pharm. 476 (1-2), 88–92. https://doi.org/10.1016/j.ijpharm.2014.09.044.

Goyanes, A., Wang, J., Buanz, A., Martínez-Pacheco, R., Telford, R., Gaisford, S., Basit, A. W., 2015. 3D Printing of Medicines: Engineering Novel Oral Devices with Unique Design and Drug Release Characteristics. Mol. Pharm. 12 (11), 4077–4084. https://doi.org/10.1021/acs.molpharmaceut.5b00510.

Simões, M.F., Pinto, R.M.A., Simões, S., 2019. Hot-melt extrusion in the pharmaceutical industry : toward filing a new drug application. Drug Discov Today. https://doi.org/10.1016/j.drudis.2019.05.013.

Goyanes, A., Allahham, N., Tren, S., Stoyanov, E., Gaisford, S., Basit, 2019. A. Direct powder extrusion 3D printing: Fabrication of drug products using a novel single-step process. 567(May). doi:10.1016/j.ijpharm.2019.118471.

Goyanes, A., Scarpa, M., Kamlow, M., Gaisford, S., Basit, A.W., Orlu, M., 2017. Patient acceptability of 3D printed medicines. Int. J. Pharm. 530 (1-2), 71–78. https://doi.org/10.1016/j.ijpharm.2017.07.064.

Brissos, S., Veguilla, M.R., Taylor, D., Balanzá-Martinez, V., 2014. The role of long-acting injectable antipsychotics in schizophrenia: A critical appraisal. Ther. Adv. Psychopharmacol. 4 (5), 198–219. https://doi.org/10.1177/2045125314540297.

de Leon, J., 2020. Personalizing dosing of risperidone, paliperidone and clozapine using therapeutic drug monitoring and pharmacogenetics. Neuropharmacology 168, 107656. https://doi.org/10.1016/j.neuropharm.2019.05.033.

Leng, D., Chen, H., Li, G., Guo, M., Zhu, Z., Xu, L.u., Wang, Y., 2014. Development and comparison of intramuscularly long-acting paliperidone palmitate nanosuspensions with different particle size. Int. J. Pharm. 472 (1-2), 380–385. https://doi.org/10.1016/j.ijpharm.2014.05.052.

Remenar, J.F., 2014. Making the leap from daily oral dosing to long-acting injectables: Lessons from the antipsychotics. Mol. Pharm. 11 (6), 1739–1749. https://doi.org/10.1021/mp500070m.

Janssen, 2017. Invega Trinza.

Darville, N., van Heerden, M., Vynckier, A.n., De Meulder, M., Sterkens, P., Annaert, P., Van den Mooter, G., 2014. Intramuscular Administration of Paliperidone Palmitate Extended-Release Injectable Microsuspension Induces a Subclinical Inflammatory Reaction Modulating the Pharmacokinetics in Rats. Pharm. Drug Deliv. Pharm. Technol. 103 (7), 2072–2087. https://doi.org/10.1002/jps.24014.

Nanaki, S., Tseklima, M., Terzopoulou, Z., Nerantzaki, M., Giliopoulos, D.J., Triantafyllidis, K., Kostoglou, M., Bikiaris, D.N., 2017. Use of mesoporous cellular foam (MCF) in preparation of polymeric microspheres for long acting injectable release formulations of paliperidone antipsychotic drug. Eur. J. Pharm. Biopharm. 117, 77–90. https://doi.org/10.1016/j.ejpb.2017.03.016.

Elmowafy, M., Alruwaili, N.K., Shalaby, K., Alharbi, K.S., Altowayan, W.M., Ahmad, N., Zafar, A., Elkomy, M., 2020. Long-Acting Paliperidone Parenteral Formulations Based on Polycaprolactone Nanoparticles; The Influence of Stabilizer and Chitosan on In Vitro Release, Protein Adsorption, and Cytotoxicity. Pharmaceutics 12 (2), 160. https://doi.org/10.3390/pharmaceutics12020160.

Stewart, S.A., Domínguez-Robles, J., McIlorum, V.J., Gonzalez, Z., Utomo, E., Mancuso, E., Lamprou, D.A., Donnelly, R.F., Larrañeta, E., 2020. Poly(caprolactone)-Based Coatings on 3D-Printed Biodegradable Implants: A Novel Strategy to Prolong Delivery of Hydrophilic Drugs. Mol. Pharm. 17 (9), 3487–3500. https://doi.org/10.1021/acs.molpharmaceut.0c00515.

Hao, W., Zheng, Z., Zhu, L., Pang, L., Ma, J., Zhu, S., Du, L., Jin, Y., 2021. 3D printing-based drug-loaded implanted prosthesis to prevent breast cancer recurrence post-conserving surgery. Asian J. Pharm. Sci. 16 (1), 86–96. https://doi.org/10.1016/j.ajps.2020.06.002.

Domínguez-Robles, J., Shen, T., Cornelius, V.A., Corduas, F., Mancuso, E., Donnelly, R.F., Margariti, A., Lamprou, D.A., Larrañeta, E., 2021. Development of drug loaded cardiovascular prosthesis for thrombosis prevention using 3D printing. Mater. Sci. Eng., C 129, 112375. https://doi.org/10.1016/j.msec.2021.112375.

Xu, X., Goyanes, A., Trenfield, S.J., Diaz-Gomez, L., Alvarez-Lorenzo, C., Gaisford, S., Basit, A.W., 2021. Stereolithography (SLA) 3D printing of a bladder device for intravesical drug delivery. Mater. Sci. Eng., C 120, 111773. https://doi.org/10.1016/j.msec.2020.111773.

Ilyés, K., Kovács, N.K., Balogh, A., Borbás, E., Farkas, B., Casian, T., Marosi, G., Tomuţă, I., Nagy, Z.K., 2019. The applicability of pharmaceutical polymeric blends for the fused deposition modelling (FDM) 3D technique: Material considerations–printability–process modulation, with consecutive effects on in vitro

release, stability and degradation. Eur. J. Pharm. Sci. 129, 110–123. https://doi.org/10.1016/j.ejps.2018.12.019.

Trivedi, R.K., Jain, P., Patel, M.C., Chatrabhuji, P.M., Trivedi, D.R., 2013. A Rapid, Stability Indicating RP-UPLC Method for Determination of Paliperidone Palmitate in a Depot Injectable Formulation 3(07) 87-92. doi:10.7324/JAPS.2013.3716.

Selmin, F., Blasi, P., DeLuca, P.P., 2012. Accelerated Polymer Biodegradation of Risperidone Poly(D, L-Lactide-Co-Glycolide) Microspheres. AAPS PharmSciTech. 13 (4), 1465–1472. https://doi.org/10.1208/s12249-012-9874-4.

Bharathi, Ch., Chary, D.K., Kumar, M.S., Shankar, R., Handa, V.K., Dandala, R., Naidu, A., 2008. Identification, isolation and characterization of potential degradation product in risperidone tablets. J. Pharm. Biomed. Anal. 46 (1), 165–169. https://doi.org/10.1016/j.jpba.2007.08.008.

Tümer, E.H., Erbil, H.Y., 2021. Extrusion-Based 3D Printing Applications of PLA Composites: A Review. Coatings 11, 1–42.

Li, D., Guo, G., Fan, R., Liang, J., Deng, X., Luo, F., Qian, Z., 2013. PLA/F68/Dexamethasone implants prepared by hot-melt extrusion for controlled release of anti-inflammatory drug to implantable medical devices: I. Preparation, characterization and hydrolytic degradation study. Int. J. Pharm. 441 (1-2), 365–372. https://doi.org/10.1016/j.ijpharm.2012.11.019.

Dissolution Methods Database | FDA. https://www.fda.gov/drugs/drug-approvals-and-databases/dissolution-methods-database. Accessed January 29, 2021.

Ruellan, A., Gratia, A., Guinault, A., et al., 2015. Bioproducts of oil industry as toughnening agents of Polylactide. Biopol 13–15.

Xie, Y., Li, G., Yuan, X., Cai, Z., Rong, R., 2009. Preparation and in vitro evaluation of solid dispersions of total flavones of Hippophae rhamnoides L. AAPS PharmSciTech. 10 (2), 631–640. https://doi.org/10.1208/s12249-009-9246-x.

Xiang, H., Wang, S., Wang, R., Zhou, Z., Peng, C., Zhu, M., 2013. Synthesis and characterization of an environmentally friendly PHBV/PEG copolymer network as a phase change material. Sci. China Chem. 56 (6), 716–723. https://doi.org/10.1007/s11426-013-4837-5.

Boetker, J., Water, J.J., Aho, J., Arnfast, L., Bohr, A., Rantanen, J., 2016. Modifying release characteristics from 3D printed drug-eluting products. Eur. J. Pharm. Sci. 90, 47–52. https://doi.org/10.1016/j.ejps.2016.03.013.

Jamróz, W., Kurek, M., Czech, A., Szafraniec, J., Gawlak, K., Jachowicz, R., 2018. 3D printing of tablets containing amorphous aripiprazole by filaments co-extrusion. Eur. J. Pharm. Biopharm. 131, 44–47. https://doi.org/10.1016/j.ejpb.2018.07.017.

Huang, S., O'Donnell, K.P., Delpon de Vaux, S.M., O'Brien, J., Stutzman, J., Williams, R. O., 2017. Processing Thermally Labile Drugs by Hot-Melt Extrusion: The Lesson with Gliclazide. Eur. J. Pharm. Biopharm. 119, 56–67. https://doi.org/10.1016/j.ejpb.2017.05.014.

Desai, D., Sandhu, H., Shah, N., Malick, W., Zia, H., Phuapradit, W., Vaka, S.R.K., 2018. Selection of Solid-State Plasticizers as Processing Aids for Hot-Melt Extrusion. J. Pharm. Sci. 107 (1), 372–379. https://doi.org/10.1016/j.xphs.2017.09.004.

Zhang, Y., Luo, R., Chen, Y., Ke, X., Hu, D., Han, M., 2014. Selection of carrier and plasticizer to improve the dissolution and bioavailability of poorly water-soluble baicalein by hot melt extrusion. AAPS PharmSciTech. 15 (3), 560–568. https://doi.org/10.1208/s12249-013-0071-x.

Yu, Y., Cheng, Y., Ren, J., Cao, E., Fu, X., Guo, W., 2015. Plasticizing effect of poly (ethylene glycol)s with different molecular weights in poly(lactic acid)/starch blends. J. Appl. Polym. Sci. 132 (16) https://doi.org/10.1002/app.41808.

Lauer, M.E., Maurer, R., De, P.AT., et al., 2018. A Miniaturized Extruder to Prototype Amorphous Solid Dispersions: Selection of Plasticizers for Hot Melt Extrusion. Pharmaceutics 10 (58). https://doi.org/10.3390/pharmaceutics10020058.

Schneider, C., Langer, R., Loveday, D., Hair, D., 2017. Applications of ethylene vinyl acetate copolymers (EVA) in drug delivery systems. J. Control. Release 262 (August), 284–295. https://doi.org/10.1016/j.jconrel.2017.08.004.

Allaf, R.M., Albarahmieh, E., AlHamarneh, B.M., 2019. Solid-state compounding of immiscible PCL-PEO blend powders for molding processes. J. Mech. Behav. Biomed. Mater. 97 (February), 198–211. https://doi.org/10.1016/j.jmbbm.2019.05.023.

de Brabander, C., van den Mooter, G., Vervaet, C., Remon, J.P., 2002. Characterization of Ibuprofen as a Nontraditional Plasticizer of Ethyl Cellulose. J. Pharm. Sci. 91 (7), 1678–1685.

Islam, M.T., Scoutaris, N., Maniruzzaman, M., Moradiya, H.G., Halsey, S.A., Bradley, M. S.A., Chowdhry, B.Z., Snowden, M.J., Douroumis, D., 2015. Implementation of transmission NIR as a PAT tool for monitoring drug transformation during HME processing. Eur. J. Pharm. Biopharm. 96, 106–116. https://doi.org/10.1016/j.ejpb.2015.06.021.

Sarpal, K., Delaney, S., Zhang, G.G.Z., Munson, E.J., 2019. Phase Behavior of Amorphous Solid Dispersions of Felodipine: Homogeneity and Drug-Polymer Interactions. Mol. Pharm. 16 (12), 4836–4851. https://doi.org/10.1021/acs.molpharmaceut.9b00731.

Bhugra, C., Telang, C., Schwabe, R., Zhong, L., 2016. Reduced crystallization temperature methodology for polymer selection in amorphous solid dispersions: Stability perspective. Mol. Pharm. 13 (9), 3326–3333. https://doi.org/10.1021/acs.molpharmaceut.6b00315.

Marsac, P.J., Li, T., Taylor, L.S., 2009. Estimation of Drug – Polymer Miscibility and Solubility in Amorphous Solid Dispersions Using Experimentally Determined Interaction Parameters. Pharm. Res. 26 (1), 40–44. https://doi.org/10.1007/s11095-008-9721-1.

Moinuddin, S.M., Ruan, S., Huang, Y., Gao, Q., Shi, Q., Cai, B., Cai, T., 2017. Facile formation of co-amorphous atenolol and hydrochlorothiazide mixtures via cryogenic-milling: Enhanced physical stability, dissolution and pharmacokinetic profile. Int. J. Pharm. 532 (1), 393–400. https://doi.org/10.1016/j.ijpharm.2017.09.020.

Manini, G., Deldime, M., Benali, S., Raquez, J.-M., Goole, J., 2021. Long-acting implantable dosage forms containing paliperidone palmitate obtained by 3D printing. Int. J. Pharm. 603 (May), 120702 https://doi.org/10.1016/j.ijpharm.2021.120702.

Grzybowska, K., Adrjanowicz, K., Paluch, M., 2016. Application of Broadband Dielectric Spectroscopy to Study Molecular Mobility in Pharmaceutical Systems. Disord. Pharm. Mater. 301–359.

Wang, B., Mathew, A., Napolitano, S., 2021. Temperature and Thickness Dependence of the Time Scale of Crystallization of Polymers under 1D Confinement. ACS Macro Lett. 10 (4), 476–480. https://doi.org/10.1021/acsmacrolett.1c00123.

Simpson, S.M., Widanapathirana, L., Su, J.T., Sung, S., Watrous, D., Qiu, J., Pearson, E., Evanoff, A., Karunakaran, D., Chacon, J.E., Kiser, P.F., 2020. Design of a Drug-Eluting Subcutaneous Implant of the Antiretroviral Tenofovir Alafenamide Fumarate. Pharm. Res. 37 (4) https://doi.org/10.1007/s11095-020-2777-2.

Kleiner, L.W., Wright, J.C., Wang, Y., 2014. Evolution of implantable and insertable drug delivery systems. J. Control. Release 181 (1), 1–10. https://doi.org/10.1016/j.jconrel.2014.02.006.

Kohno, M., Andhariya, J.V., Wan, B.o., Bao, Q., Rothstein, S., Hezel, M., Wang, Y., Burgess, D.J., 2020. The effect of PLGA molecular weight differences on risperidone release from microspheres. Int. J. Pharm. 582, 119339. https://doi.org/10.1016/j.ijpharm.2020.119339.

Rawat, A., Stippler, E., Shah, V.P., Burgess, D.J., 2011. Validation of USP apparatus 4 method for microsphere in vitro release testing using Risperdal Consta. Int. J. Pharm. 420 (2), 198–205. https://doi.org/10.1016/j.ijpharm.2011.08.035.

Shen, J., Lee, K., Choi, S., Qu, W., Wang, Y., Burgess, D.J., 2016. A reproducible accelerated in vitro release testing method for PLGA microspheres. Int. J. Pharm. 498 (1–2), 274–282. https://doi.org/10.1016/j.ijpharm.2015.12.031.

Bode, C., Kranz, H., Fivez, A., Siepmann, F., Siepmann, J., 2019. Often neglected: PLGA/PLA swelling orchestrates drug release: HME implants. J. Control. Release 306 (May), 97–107. https://doi.org/10.1016/j.jconrel.2019.05.039.

Khaled, S.A., Alexander, M.R., Irvine, D.J., Wildman, R.D., Wallace, M.J., Sharpe, S., Yoo, J., Roberts, C.J., 2018. Extrusion 3D Printing of Paracetamol Tablets from a Single Formulation with Tunable Release Profiles Through Control of Tablet Geometry. AAPS PharmSciTech. 19 (8), 3403–3413. https://doi.org/10.1208/s12249-018-1107-z.

Elbadawi, M., Muñiz Castro, B., Gavins, F.K.H., Ong, J.J., Gaisford, S., Pérez, G., Basit, A. W., Cabalar, P., Goyanes, A., 2020. M3DISEEN: A novel machine learning approach for predicting the 3D printability of medicines. Int. J. Pharm. 590, 119837. https://doi.org/10.1016/j.ijpharm.2020.119837.

Muñiz Castro, B., Elbadawi, M., Ong, J.J., Pollard, T., Song, Z., Gaisford, S., Pérez, G., Basit, A.W., Cabalar, P., Goyanes, A., 2021. Machine learning predicts 3D printing performance of over 900 drug delivery systems. J. Control. Release 337, 530–545. https://doi.org/10.1016/j.jconrel.2021.07.046.

Bhardwaj, U., Burgess, D.J., 2010. A novel USP apparatus 4 based release testing method for dispersed systems. Int. J. Pharm. 388 (1–2), 287–294. https://doi.org/10.1016/j.ijpharm.2010.01.009.

Andhariya, J.V., Shen, J., Wang, Y., Choi, S., Burgess, D.J., 2019. Effect of minor manufacturing changes on stability of compositionally equivalent PLGA microspheres. Int. J. Pharm. 566 (June), 532–540. https://doi.org/10.1016/j.ijpharm.2019.06.014.